






Article

Photocatalytic Oxygenation of Heterostilbenes—Batch versus Microflow Reactor

Milena Mlakić ^{1,†} , Anita Šalić ^{2,†} , Matea Bačić ², Bruno Zelić ² , Ivana Šagud ³, Ottó Horváth ^{4,*} 
and Irena Škorić ^{1,*} 

- ¹ Department of Organic Chemistry, Faculty of Chemical Engineering and Technology, University of Zagreb, Marulićev trg 19, HR-10000 Zagreb, Croatia; mdragojev@fkit.hr
- ² Department of Reaction Engineering and Catalysis, Faculty of Chemical Engineering and Technology, University of Zagreb, Marulićev trg 19, HR-10000 Zagreb, Croatia; asalic@fkit.hr (A.Š.); mbacic@fkit.hr (M.B.); bzelic@fkit.hr (B.Z.)
- ³ Teva api Chemical R&D, Pliva, Prilaz Baruna Filipovića 25, HR-10000 Zagreb, Croatia; Ivana.Sagud@pliva.com
- ⁴ Center for Natural Sciences, Department of General and Inorganic Chemistry, Faculty of Engineering, University of Pannonia, P.O. Box 1158, H-8210 Veszprém, Hungary
- * Correspondence: horvath.otto@mk.uni-pannon.hu (O.H.); iskoric@fkit.hr (I.Š.); Tel.: +36-88-624-000 (ext. 6049) (O.H.); +385-1-4597-241 (I.Š.)
- † These authors contributed equally.

Abstract: On the basis of earlier results with furan and thiophene derivatives of benzobicyclo[3.2.1]octadiene, photocatalytic oxygenation of novel furo- and thieno heterostilbenes with water-soluble manganese(III) porphyrins offered suitable possibilities to study their reactivities and reaction pathways depending on the heteroatom and the catalyst charge. The experiments were carried out in two reactors types (batch and microflow) to investigate the geometric effects. NMR spectroscopy, GC, and UPLC/MS analyses were applied for identification and quantification of the products. As our results indicated, the 2-thienyl and the common *p*-tolyl groups in the starting compounds remained intact due to their stronger aromaticity. Hence, the thieno derivative underwent oxygenation only at the open-chain part of the molecule, and the rates of its reactions were much lower than those of the furyl analogue. The less stable furan ring was easily oxygenated, its products with highest ratios were 2-furanon derivatives. Epoxide formation occurred at the open-chain parts of both substrates preferably by the anionic catalyst. Nevertheless, the conversion rates of the substrates were higher with the cationic porphyrin, according to electrophilic attacks by photogenerated Mn(V)=O species. Additionally, the reactions were significantly faster in microflow reactors due to the more favorable circumstances of mass transfer, diffusion, and light penetration.

Keywords: heterostilbenes; water-soluble manganese(III) porphyrins; photocatalytic oxygenation; thiophene; furan; reactor types



Citation: Mlakić, M.; Šalić, A.; Bačić, M.; Zelić, B.; Šagud, I.; Horváth, O.; Škorić, I. Photocatalytic Oxygenation of Heterostilbenes—Batch versus Microflow Reactor. *Catalysts* **2021**, *11*, 395. <https://doi.org/10.3390/catal11030395>

Academic Editors: Raffaele Molinari and Cristina Lavorato

Received: 26 February 2021

Accepted: 18 March 2021

Published: 20 March 2021

Publisher's Note: MDPI stays neutral with regard to jurisdictional claims in published maps and institutional affiliations.



Copyright: © 2021 by the authors. Licensee MDPI, Basel, Switzerland. This article is an open access article distributed under the terms and conditions of the Creative Commons Attribution (CC BY) license (<https://creativecommons.org/licenses/by/4.0/>).

1. Introduction

In recent years, numerous research groups in the field of organic synthetic chemistry put their focus on photochemistry as a relatively young science. Light as the main reagent in photochemical reactions opens pathways to interesting photochemical products. Nowadays, trends for the synthesis of new photoproducts include various innovative photocatalysts with nanoparticles such as palladium nanoparticles [1]. Additionally, very promising results are obtained by reactions in which porphyrin complexes coordinated with certain metals are used as catalysts; therefore, scientists have studied a whole range of metals within porphyrin structures as well as their advantages in various catalytic oxidations [2]. There are examples of porphyrin complexes coordinated with ruthenium [3]. Manganese porphyrins have already been used in the past for various organic reactions. A great example for that kind of application is the synthesis of stilbene molecules in a

microwave reactor, using hydrogen peroxides [4]. There are a number of other reactions in which different photocatalysts are used, such as hydroacylation and diacylation reactions [5], Heck cross-coupling reactions, and various isomerizations [6]. Photocatalytic oxygenations using various photocatalysts such as nanoparticles containing cadmium sulfite and green lamps are also known in the literature [7]. Blue LED lamps have been applied in photocatalytic isomerizations of various stilbene derivatives [8]. Photocatalytic reactions on styrenes, cyclohexenes, and stilbenes, using a cobalt-based metal–organic framework, are also known. Transition metal ions act as active species for high selectivity of epoxidation reactions [9]. During those photocatalytic reactions, a double bond is broken under the influence of light and a certain photocatalyst, resulting in formation of new photooxygenation products, which in most cases belong to the group of epoxides, alcohols, and/or formyl derivatives.

In order to enhance process efficiency, there is a trend towards replacement of batch reactors with flow reactors for photochemical reactions. Microflow reactors are one of flow reactor types, whose main characteristic is the microdimension (channel diameter up to 500 μm). In comparison with meso- and macroflow reactors, they significantly contribute to all positive effects of the flow reactor usage. A large surface-to-volume ratio, a short diffusion path, and fast and efficient mass and heat transfer are just some of the most important advantages of microflow reactor systems that have successfully been applied in the field of flow organic synthesis. These systems are usually characterized by a higher conversion and productivity compared with reactions carried out in conventional reactor systems. The application of microflow reactors in organic photochemical synthesis has been present for some time now [10,11]. Photocycloaddition, photoisomerization, cyclization, decarboxylation [12], and click reactions [13] have already been successfully performed in different microsystems. Additionally, very small dimensions of microreactors allow more efficient and homogeneous use of light irradiation throughout the reaction mixture. As a result of their application, a significant shift in photochemical synthesis [12] can be noticed. In this way, the reactions are often accelerated and the processes that are carried out in the batch reactor for hours/days in microreactors can be performed in a few seconds/minutes. Reduction of the reaction time also minimizes the formation of different by-products and increases the overall productivity of the process.

In our laboratory, a simple and efficient protocol is utilized for the synthesis of functionalized benzobicyclo[3.2.1]octenes/octadienes (Figure 1E,F) from organic substrates (A–C) having no characteristic functional groups other than reactive double bonds [14–18]. Utilization of anionic and cationic manganese(III) porphyrins (Figure 2) as photocatalysts resulted in the formation of epoxy or hydroxy derivatives as main products on the reactive double bonds of the furan or thiophene rings or on the free double bond, as well as other minor photooxygenation products.

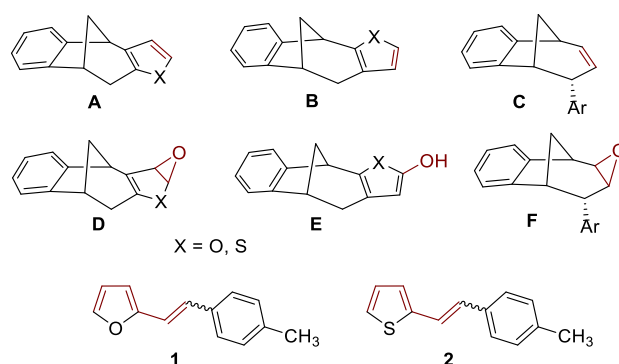


Figure 1. Structures of previously investigated substrates (A–C), their main photooxygenated products (D–F) [17], and structures of heterostilbenes 1 and 2 as new substrates for photocatalytic oxygenation reactions.

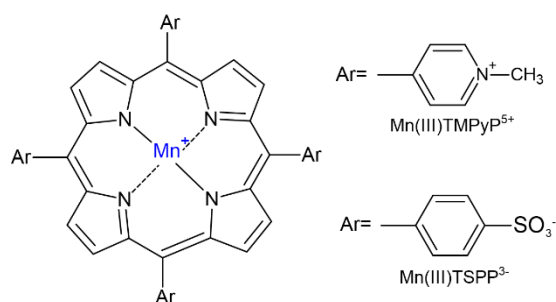


Figure 2. Structures of manganese(III) complexes with cationic 5,10,15,20-tetrakis(1-methyl-4-pyridinium)porphyrin (Mn(III)TMPyP⁵⁺) and anionic 5,10,15,20-tetrakis(4-sulfonatophenyl) porphyrin (Mn(III)TSPP^{3−}).

These results demonstrated that the charge on the porphyrin ligand or pH determines the pathway of the oxygenation reaction in this system, offering the possibility of controlling the types and distributions of the final products. Additionally, the application of water-soluble metalloporphyrins for oxygenation of organic substrates in water–acetone solvent mixture promotes the easy separation of the products from the catalyst, ensuring the efficient reuse of the latter one. This feature is a considerable advantage over the fully hydrophobic systems.

In air- or oxygen-saturated solutions, free-base porphyrins generate only singlet oxygen in these photocatalytic reactions, while metalloporphyrins can be involved in other light-induced processes, producing species with higher oxidation potential than that of ¹O₂. Application of manganese(III) porphyrins well demonstrated this diversity. In most of these processes, the first reaction step of the (triplet) excited-state complex was an electron transfer. These reactions produce directly or indirectly Mn(IV) then Mn(V) porphyrins as intermediates playing important roles in the oxygenation processes. This has been exemplified in earlier works [19,20] and more recent studies [21–23], regarding the photocatalytic oxygenation of cyclohexene. In aqueous systems, photo-induced homolysis of the bond between the metal center and chloride or hydroxide axial ligands led to the formation of (P)Mn^{IV}=O [24,25]. The oxidized ligand (Cl[•] or HO[•]) is a very reactive oxidative agent, and the Mn(II) species formed in this reaction undergoes an oxidation with the dissolved O₂. The Mn(IV) complexes formed disproportionate, producing highly reactive manganese(V)-oxo species (along with the starting Mn(III) complex). In the oxo derivatives, the oxygen atom coordinated with a double bond is located in an axial position, increasing the oxidation state of the metal center by two, leading to Mn(IV) and Mn(V). The rate constants for epoxidation of olefins are several orders of magnitude higher for manganese(V)-oxo porphyrins than for the corresponding Mn(IV) species. Hence, (P)Mn^V=O can be considered as the major oxidant in the photocatalytic oxygenations in these systems. Nevertheless, in some cases, the (P)Mn^{IV}=O complexes can also result in direct hydrogen abstraction from hydrocarbon moiety [26]. On the basis of the preliminary pieces of information summarized above, the aim of our work was to study photocatalytic oxygenations of analogous furo- and thieno heterostilbenes with water-soluble manganese(III) porphyrins (Figure 2), to reveal how their reactivities and reaction pathways depend on the heteroatom and the catalyst charge. Such heterostilbenes were chosen as starting substrates in this work because their photocatalytic oxygenation can provide new functionalized molecules similar to the structure of the well-known natural stilbenoid phenol resveratrol. Additionally, two types of reactors (batch and microflow) were applied for these experiments to compare the effects of the geometric differences on the reaction rates.

2. Results and Discussion

In this research, furo- (1) and thienostilbenes (2) (Figure 1), as new substrates with differently reactive double bonds, have been chosen for photooxygenation reactions to see if the more conjugated heteroaromatic systems change the reactivity and selectivity of the

oxygenated processes in comparison with previously investigated systems. Differences and similarities in these pathways may shed light on the mechanisms of the oxygenation processes of heterostilbenes **1** and **2**, giving hints for appropriate choice of the catalyst and on other conditions to achieve efficient conversion with high selectivity. The charge on the ligand, influencing its Lewis basicity, may affect the catalytic activity of the complex through the metal center. Selected reactions were performed in a batch reactor (50 cm³ cylindrical photoreactor) as presented in Figure 3a.

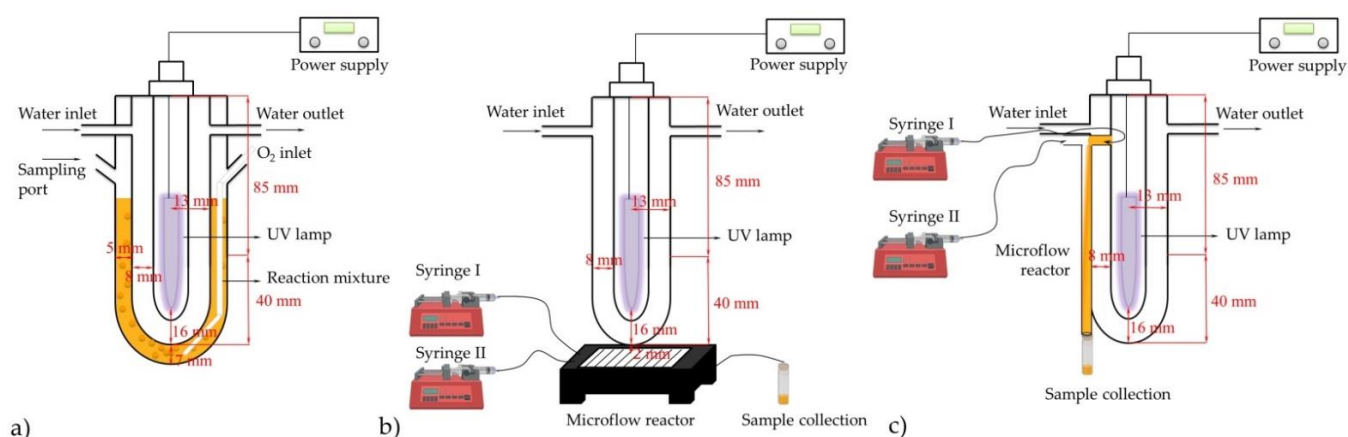


Figure 3. Experimental set-up for photocatalytic oxygenation performed in a (a) batch reactor, (b) winding geometry microflow reactor, and (c) straight channel microflow reactor.

In order to get more information about the kinetic mechanism of photochemical conversion of both selected substrates, reaction rates were estimated. According to Harris and Keshwani [27], for any given chemical reaction, the kinetic mechanism refers to the sequence of elementary steps by which the overall chemical change occurs. Additionally, by knowing the mechanism, a formation time, from substrate to product, can be defined.

A step forward in a research was made by shifting the process from batch to a microflow reactor. A total of four different tubular microflow reactors (one with winding geometry (Figure 3b) and three with straight microchannel (Figure 3c) were studied and compared based on substrate conversion, products formed, and reaction time.

2.1. Synthesis and Identification of Photooxygenation Products

Starting substrates, compounds **1** and **2** as mixtures of *cis*- and *trans*-isomers, were obtained in the Wittig reaction (isolated yields for compound **1**: 83%; for compound **2**: 88%; according to the integrals in UPLC analyses and ¹H NMR spectra, the ratio of isomers of compound **1** was *cis*:-*trans*- = 1:1.3, and for compound **2** the ratio of isomers was *cis*:-*trans*- = 1:1.2) starting from phosphonium salt prepared in the laboratory and corresponding heterocyclic aldehydes distilled under low pressure. The presence of both isomers of **1** and **2** were successfully detected by UPLC analysis (Figure 4). Photocatalytic oxygenation reactions of **1** and **2** were performed in air-saturated acetone/water (50/50%) mixture in the presence of Mn(III)TMPyP⁵⁺ or Mn(III)TSPP³⁻ as photocatalyst. In order to obtain the best yield of the isolated products, the reaction time was varied from 2 h to 16 h, combined with changing the charge of the photocatalyst and the concentration of the substrates.

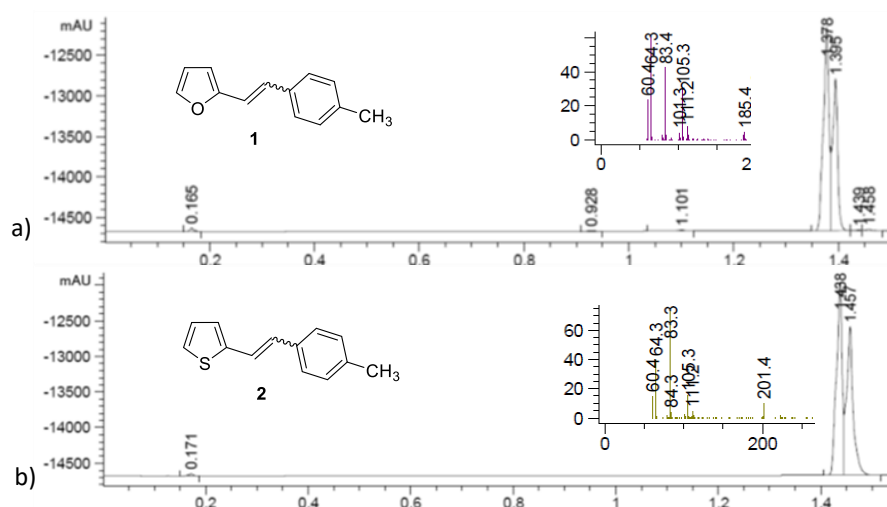
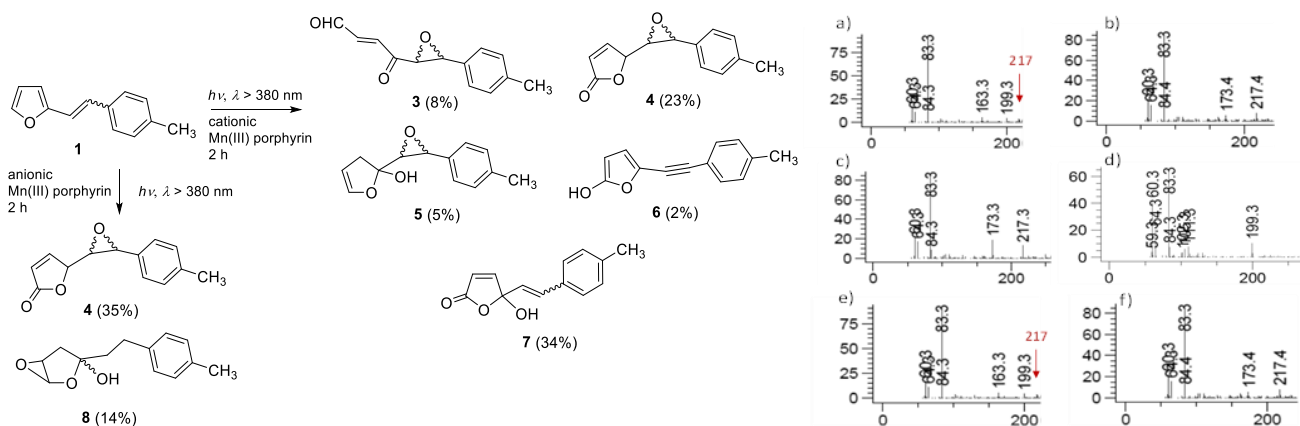
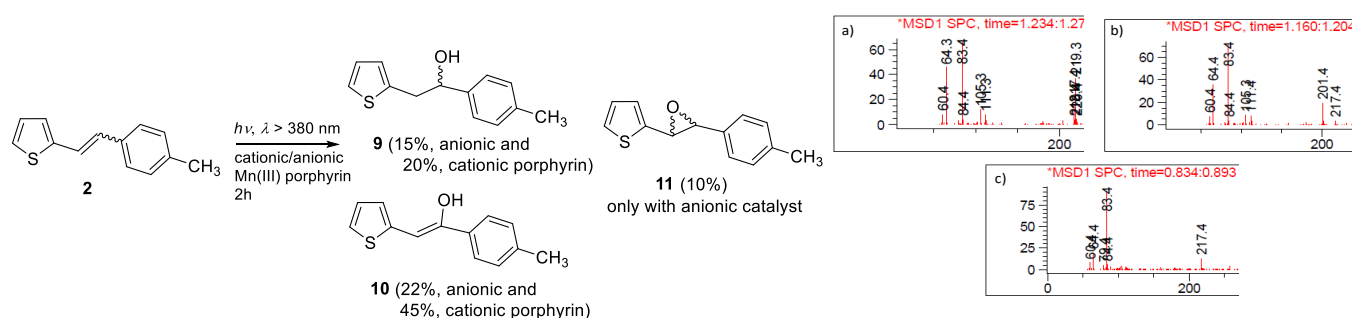


Figure 4. DAD chromatograms of the mixture of isomers of the starting furyl derivative **1** (a) and thienyl derivative **2** (b) along with the retention times and mass spectra.

The most characteristic results obtained under various conditions are demonstrated by Schemes 1 and 2. These clearly indicate that the nature of the heteroatom can drastically affect the reaction course, leading to significantly deviating types of products, in which oxygenation took place on different parts of the unsaturated skeleton. According to ^1H NMR spectra, GC and UPLC/MS analyses of the reaction mixtures obtained during photocatalytic oxygenation under different reaction conditions, in the case of furyl derivative **1**, using anionic (Mn(III)TSPP^{3-}) or cationic (Mn(III)TMPyP^{5+}) porphyrins, six new photoproducts were detected (Scheme 1), while three photoproducts were observed in the case of the thienyl substrate **2** (Scheme 2).



Scheme 1. Reaction pathway and product ratios for the photocatalytic oxygenation of **1** in air-saturated system at pH 7, using cationic/anionic Mn(III) porphyrins, together with mass spectra obtained in the experiment using cationic Mn(III) porphyrin at the following retention times: 0.908' (a) for **5**, 0.946' (b) for **4**, 1.012' (c) for **3**, 1.175' (d) for **6**, and 1.278' (f) for **7**; and using anionic Mn(III) porphyrin at 0.824' (e) for **8**.



Scheme 2. Reaction pathways and product ratios for the photocatalytic oxygenation of **2** in air-saturated system at pH 7, using cationic or anionic Mn(III) porphyrins, together with mass spectra obtained on the UPLC/MS system for thienyl photooxygenation products **9** (a), **10** (b), and **11** (c) with the corresponding retention times.

Concerning the results obtained for the furyl derivative **1**, all the photoproducts, **3–8** (Scheme 1), were isolated by repeated column and thin-layer chromatography and characterized by spectroscopic methods. From the ^1H NMR spectra and UPLC/MS analyses, taking our previous results [14,17,18] as reference, the structures of all the new compounds were determined. Molecular ions m/z 216 (**3–5**, **7**, **8**) and m/z 198 (**6**) indicated that one or two oxygen atoms were incorporated in the starting substrate **1**, having masses 32 or 14 higher than the mass for **1** with m/z 184 (Scheme 1). All the photoproducts have recognizable patterns in their ^1H NMR spectra (Figures 5 and 6), but different numbers of signals in their aliphatic or unsaturated regions, existence or not of the characteristic furyl coupling constants, characteristic signals for double bonds, signal for the formyl or hydroxyl groups, depending on the structure. These suggested results were confirmed by IR spectra providing also characteristic signals for the formyl, keto, and hydroxy functional groups.

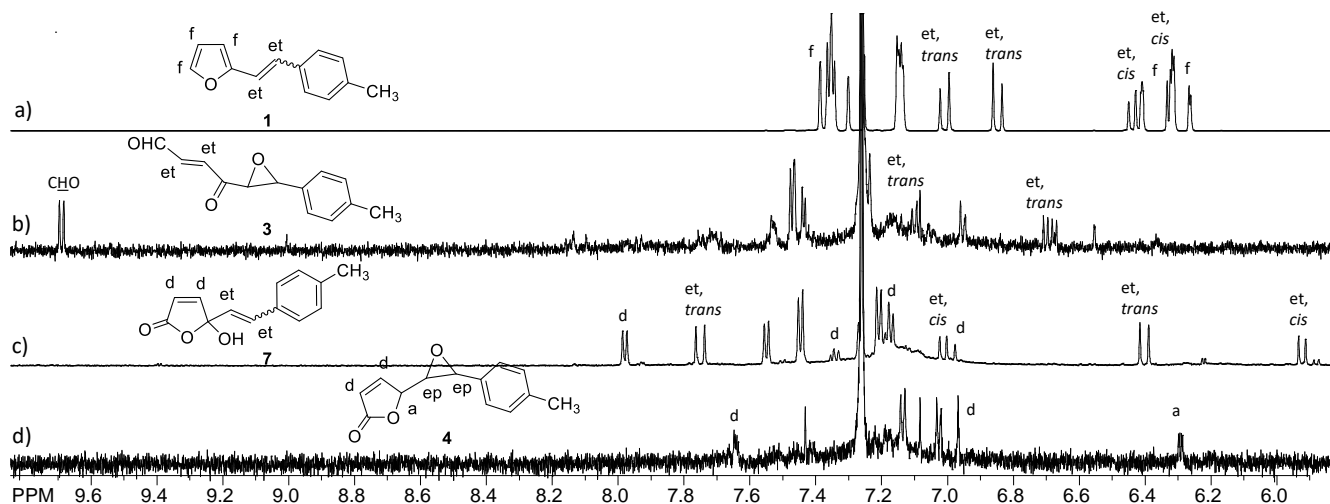


Figure 5. Partial ^1H NMR spectra (CDCl_3) of starting compound **1** (a), formyl derivative **3** (b), unsaturated carbonyl compound **7** (c), and epoxy structure **4** (d) with characteristic patterns for assignment of the products' structure.

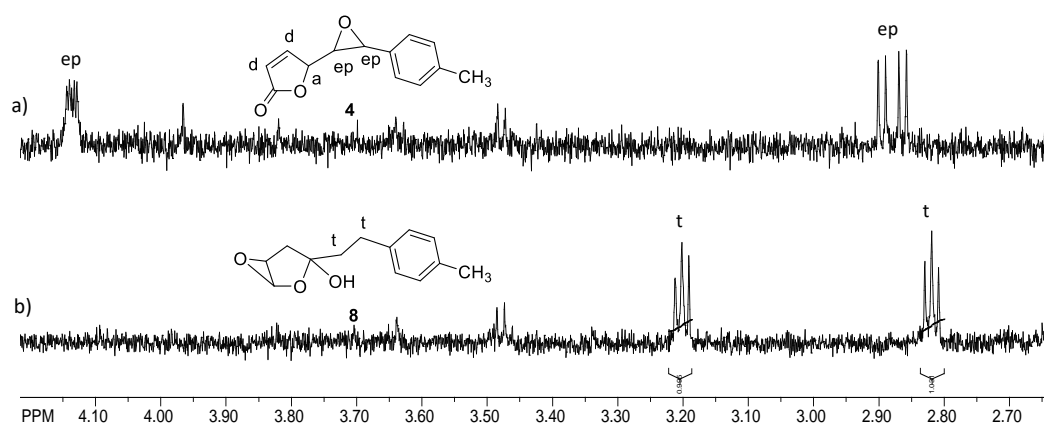


Figure 6. Aliphatic parts of ^1H NMR spectra (CDCl_3) of products **4** (a) and **8** (b) with characteristic patterns for assignment of the specific structures.

Photooxygenated products **4** and **8** show the characteristic aliphatic part of the NMR spectra with three signals with the ratio of integrals of 1:1:1 (**4**) or two triplets, which correspond to two methylene groups (**8**) (Figure 6). In the ^1H NMR spectrum of photoproduct **8**, also the integral of four protons at about 2 ppm can be found beside the signal of the methyl group. All these pieces of information together with the masses of six products (**3–8**), confirmed by UPLC/MS analysis, clearly show the tendency of the starting furostilbene **1** under the conditions of photooxygenation using Mn(III) porphyrins and the reactivity of the furan ring. In addition to these isolated products, several additional products were detected in traces in the enriched fractions, with characteristic signals in the proton NMR indicating the existence of some formyl or epoxy derivatives.

Thienostilbene **2** (as a mixture of *cis*- and *trans*-isomers, Figure 4), using cationic or anionic metallated porphyrins during photooxygenation reaction, gave three characteristic photoproducts, **9–11** (Scheme 2). All of them were isolated by repeated column and thin-layer chromatography and characterized by spectroscopic methods. From the ^1H NMR spectra and UPLC/MS analyses the structures of all the obtained photoproducts, **9–11**, were successfully assigned. Molecular ions m/z 218 (**9**) and m/z 216 (**10** and **11**) indicated that in all cases, only one oxygen atom was incorporated in the structure of the starting substrate **2** (Scheme 2). For **9**, the fragment with mass m/z 216 is two units lower than the base peak (m/z 218) belonging to the molecular ion.

It is important to emphasize that product **11** is isolated only in the case of anionic photocatalysts (Scheme 2). As the forming of the hydroxylated structures can be explained by cleavage of the epoxide ring, it can be supposed that in the case of cationic porphyrin, product **11** is just an intermediate. It can be concluded that in the case of thienostilbene **2**, the types of the photoproducts are the same independently of the photocatalysts used, but the isolated yields differ.

Photoproducts **9–11** also have very recognizable patterns in their ^1H NMR spectra (Figures 7 and 8). The main photoproduct in both cases is compound **10** (Scheme 2), with all aromatic signals in the proton NMR (Figure 6b) shifted in comparison with the signals of the starting substrate **2** (Figure 7a). The characteristic coupling constants for three protons on the thiophene ring are well recognizable, confirming the nonreactivity of the thiophene ring in the reaction. Additionally, this stability is confirmed by the structures of photoproducts **9** and **11** (Figure 8), where the thiophene ring remained intact again. IR spectra of **9** and **10** confirmed the existence of hydroxyl groups in the structures.

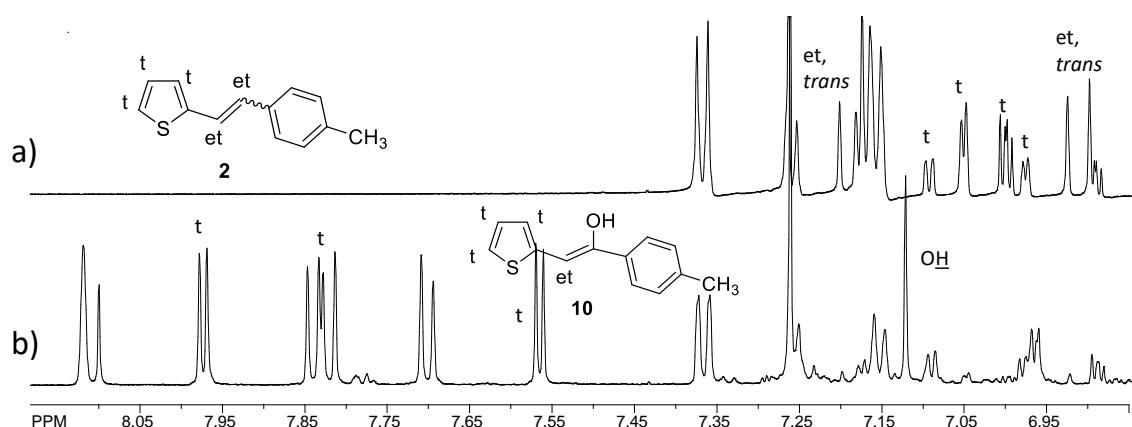


Figure 7. Aromatic parts of ^1H NMR spectra (CDCl_3) of the starting thienyl derivative **2** (a) and the major photooxygenation product **10** (b) with characteristic pattern for assignment of the specific structures.

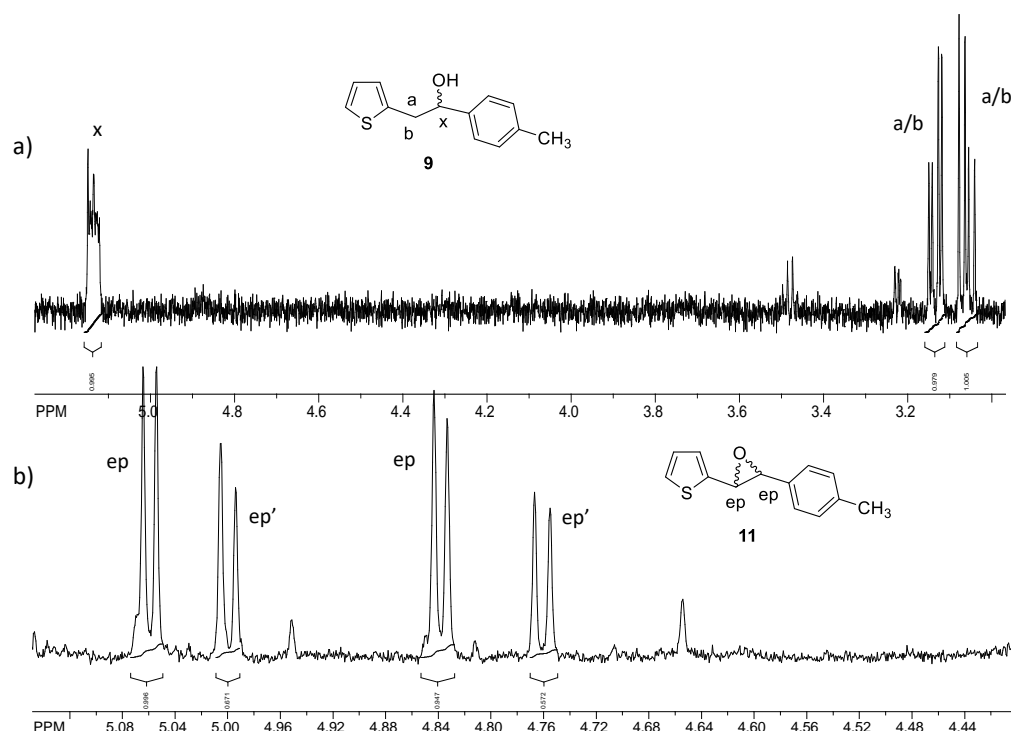


Figure 8. Aliphatic parts of ^1H NMR spectra (CDCl_3) of hydroxy ABX system in product **9** (a) and epoxy derivative **11** (b), as mixture of diastereomers in the ratio 1:1.5 with characteristic patterns for assignment of the specific structures.

Compounds **9** and **11** have ^1H NMR spectra with patterns of their aliphatic protons that are distinguishable and differ from the pattern of the starting compound **2** and photo-product **10** (Figure 8). In the case of **9**, the protons of hydroxy ABX system (Figure 8a) very clearly refer to the assigned structure of the hydroxylated photoproduct without a double bond in the structure, except those in the thiophene and aryl rings. Epoxy derivative **11** is obtained as a mixture of two stereoisomers with characteristic pairs of doublets in the ^1H NMR spectrum between 5.1 and 4.7 ppm and appropriate ratio of integrals for the protons on the epoxy ring (Figure 8b).

The results regarding the structures and ratios of the products obtained by the photocatalytic oxygenation of analogous furyl and thienyl derivatives are suitable for reasonable comparisons in the respects of both the type of the heteroatom and the charge of the cata-

lyst. The tendencies observed through these comparisons can be appropriately interpreted based of the general characteristics of the reaction mechanisms and the substrates involved.

No matter which combination of substrate and catalyst was applied, the *p*-tolyl group remained intact in each product. This is probably the consequence of its high stability due to the strong aromatic character. Similarly, in the case of the thiophene derivatives, the 2-thienyl group proved to be inert, indicating its appreciable aromaticity. Deviating from these moieties, the 2-furyl group was easily transformed, as seen in each product originated from **1**. Moreover, only one product kept the aromatic furan ring (as a hydroxylated one, **6**), the transformation ceased the aromaticity of this heterocycle in the other cases. These results confirm that the aromatic character of furan is much weaker than that of thiophene, in accordance with our earlier observations in similar systems [16,18].

As a consequence of the deviating reactivities, photocatalytic oxygenation of the furyl derivative (**1**) provided more types of products in the presence of the cationic catalysts than the analogous thienyl derivative (**2**) did. Hence, lower reactivity resulted in higher selectivity. Accordingly, as indicated above, oxygenation took only place on the open-chain part of the thienyl products. Between the two hydroxy derivatives (**9** and **10**), which were produced by application of both cationic and anionic catalysts, the ratio of the one keeping the double bond (**10**) was significantly higher in each case. It is reasonable because the chance for saturation of a double bond is less probable in the case of an electrophilic attack. Moreover, the ratios obtained by the cationic porphyrin were higher for both products than those gained by the anionic catalyst. These values are also in accordance with the crucial role of electrophilicity of the reactive agent, most likely Mn(V) porphyrin, in these oxygenations because this feature is significantly stronger for the cationic than for the anionic catalyst. Interestingly, the epoxy-type product **11** was formed only in the presence of the anionic porphyrin. According to earlier observations [16], epoxides may be precursors of corresponding hydroxy derivatives in such oxygenations by the cationic catalyst, hence, they can be end-products in the presence of the less reactive anionic Mn(V) porphyrin even after a 16 h irradiation.

Since the photooxygenations of the more reactive furyl derivative (**1**) were realized by only 2 h irradiations, epoxides on the open-chain parts were also produced by both catalysts. Derivative **4** was formed in both cases, but with a higher ratio (35%) in the presence of the anionic porphyrin. The ratios of the epoxide products obtained by the cationic catalyst were significantly lower, suggesting their intermediate role. No matter which porphyrin was applied for the oxygenation of **1**, the products with the highest ratios were 2-furanon derivatives (**4** and **7**), indicating that a stronger oxidation was preferred in this position on the furan ring. Accordingly, the ratios of the less oxidized hydroxy derivatives (**5** and **6**) were only 5% and 2%, respectively. Even the open-ring product (**3**) was formed in a higher amount. The only product epoxidized on the furan ring (**8**) was obtained by the anionic porphyrin in an appreciable ratio, also indicating its intermediate character. The higher reactivity of the furyl derivative in these oxygenation processes is also demonstrated by the incorporation of two oxygen atoms in most of its products, while those originated from **2** contained only one O.

2.2. Kinetics

In order to estimate the rate constant (*k*) of selected reactions, a total of 11 experiments were performed in a batch reactor (Table 1). A reaction rate constant represents a relationship between the reaction rate and the initial concentration for a specific substrate. Therefore, it was necessary to determine the reaction rates (*r*) for selected substrates. Reaction rate ($\text{mol dm}^{-3} \text{ h}^{-1}$), i.e., the speed at which a chemical reaction proceeds, was calculated from experimental results as the amount of the substrate consumed in a unit of time. As shown in Table 1, higher initial concentrations of substrate, *c* (at a constant catalyst concentration, *c*_{cat}), lead to higher reaction rates. On the basis of the calculated reaction rates for different initial concentrations of substrate, the reaction rate constant was estimated. It was noticed that all investigated reactions followed first-order kinetics (data not

shown). Based on the reaction rate constants, the furyl derivate proved to be more reactive than the thienyl one, as already demonstrated. Additionally, reactions carried out with the cationic catalyst were slower than those performed with the anionic porphyrin (Table 1).

Table 1. Reaction rates and rate constants of selected reactions.

Catalyst	Substrate (S)	c (mol dm ⁻³)	c_{cat} (mol dm ⁻³)	r (mol dm ⁻³ h ⁻¹)	Confidence Interval	k (h ⁻¹)
Cationic	1	0.00113	11×10^{-5}	8.61×10^{-5}	8.31×10^{-6}	0.045
	1	0.00225	11×10^{-5}	1.38×10^{-4}	1.05×10^{-5}	
	1	0.00450	11×10^{-5}	1.36×10^{-4}	1.69×10^{-5}	
	2	0.00120	11×10^{-5}	1.59×10^{-3}	1.19×10^{-4}	1.338
	2	0.00245	11×10^{-5}	1.55×10^{-3}	4.29×10^{-4}	
	2	0.00490	11×10^{-5}	7.17×10^{-3}	6.02×10^{-4}	
Anionic	1	0.00113	9.8×10^{-5}	5.56×10^{-5}	9.57×10^{-7}	0.052
	1	0.00225	9.8×10^{-5}	1.04×10^{-4}	1.41×10^{-5}	
	1	0.00450	9.8×10^{-5}	2.50×10^{-4}	5.79×10^{-5}	
	2	0.00120	9.8×10^{-5}	2.83×10^{-3}	7.14×10^{-4}	1.503
	2	0.00245	9.8×10^{-5}	9.93×10^{-3}	2.60×10^{-4}	
	2	0.00490	9.8×10^{-5}	6.57×10^{-3}	6.53×10^{-4}	

2.3. Synthesis in Microflow Reactors

As mentioned earlier, photocatalytic oxygenation reactions were firstly performed in a batch reactor. Both substrates (1 and 2) and both catalysts (cationic and anionic) were tested under different initial concentrations, and the results obtained were compared based on the reaction rates (r) and the rate constants (k). Changes in the conversions for two selected reactions are presented in Figure 9a. The experiments were conducted under the following initial conditions: first reaction: $c(1) = 0.00225$ mol dm⁻³ and $c_{catalytic} = 11 \times 10^{-5}$ mol dm⁻³; second reaction: $c(2) = 0.00245$ mol dm⁻³ and $c_{anionic} = 9.8 \times 10^{-5}$ mol dm⁻³. As it can be seen from the data shown in Figure 9a, the reaction, using cationic catalyst and 1 as substrate, was significantly slower than the one where reaction of 2 as substrate was catalyzed with anionic catalyst. The same is evident from kinetic data if reaction rates and rate constants are compared (Table 1). Complete conversion was observed after 2 h for substrate 2 and after 16 h for substrate 1, respectively.

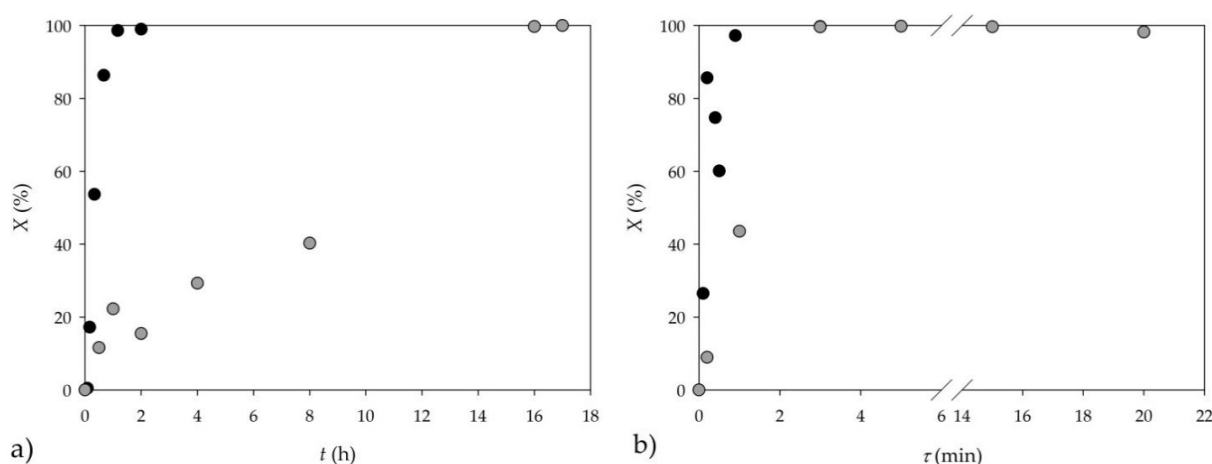


Figure 9. Comparison of the photocatalytic oxygenation process performed in (a) a batch reactor and (b) a winding channel geometry microflow reactor (• thienyl (1) and • furyl (2) as substrate).

A step forward in a process development was made by replacing batch with microflow reactors. A total of four different tubular microflow reactors were studied and compared with results obtained in a batch reactor, based on substrate conversion, formed products, and reaction time. The obtained results are summarized in Table 2 and Figure 9b. The reac-

tions were significantly accelerated in microflow reactors, where the complete conversions for substrates **1** and **2** were observed for residence times of 3.5 and 0.7 min, respectively (Figure 9b).

Table 2. Comparison of conversions obtained in different microflow reactors for the residence time of $\tau = 0.2$ min.

Microflow Reactor Geometry		Reaction	
		$c(1) = 0.00225 \text{ mol dm}^{-3}$ $c_{\text{cationic}} = 11 \times 10^{-5} \text{ mol dm}^{-3}$	$c(2) = 0.00245 \text{ mol dm}^{-3}$ $c_{\text{anionic}} = 9.8 \times 10^{-5} \text{ mol dm}^{-3}$
		X (%)	X (%)
Winding channel		8.92	85.66
Streight channel	I.	4.84	82.49
	II.	4.61	81.64
	III.	3.89	80.94

Channel dimensions and geometry have the influence on the conversion for the same residence time ($\tau = 0.2$ min, Table 2). By decreasing the channel width, the conversion is increasing (Table 2), probably due to the increased surface-to-volume ratio, the shorter diffusion path, and the homogeneous use of light irradiation throughout the reaction mixture.

From the analyses of UPLC chromatograms, mass spectra and results of gas chromatography of the samples obtained after complete conversion in the microreactor (Figure 9b), the presence of products **4**, **6**, **7**, and **8** (starting from **1**) and **9**, **10**, and **11** (starting from **2**) can be confirmed, but not all of them in all experiments and with various distributions depending on the residence time. The additional proof of these products is the comparison of their retention times and masses with those obtained for the signals from the batch reactions of compounds **1** and **2**.

Beside the identified products in the experiments performed in the microreactor, a new signal in UPLC/MS analysis appeared at 0.152' with m/z 32 higher than for starting furyl substrate **1**. In the case of the thienyl derivative **2**, a new signal at 0.274' with m/z 217 was also detected in comparison with the batch experiment. The difference in the distribution of the photooxygenation products between batch and flow experiments is not surprising due to advantages emerging from the reduction in the dimension of the microchannel. According to Cambié et al. [28], a narrower channel allows more efficient and homogeneous use of light irradiation throughout the reaction mixture. Consequently, the reactions are often accelerated, as clearly demonstrated in this research, too. Reduction of the reaction time minimizes the formation of different byproducts and increases the overall productivity of the process. Improved reaction selectivity and increased reproducibility of photochemical reactions performed in microflow reactors are shown elsewhere [29–33].

2.4. Calculations

For comparison of results obtained from different reactor arrangements, the reaction or residential times were determined during which the number of photons absorbed by a unit of volume of the irradiated solutions were approximately the same in each system. Such calculations take the emission spectrum of the light source and the absorption spectrum of the photocatalyst into account. Considering the overlap of these spectra and the individual geometrical arrangements, the fractions of the emitted light absorbed by the photoactive species (a porphyrin in this case) can be determined for each reactor. The photon flux absorbed by the solution of the catalyst solution in the overlapping range of the spectra (between λ_1 and λ_2) can be expressed by the following equation (Equation (1)):

$$I_{abs} = \int_{\lambda_1}^{\lambda_2} I_0(\lambda) (1 - 10^{-A(\lambda)}) d\lambda \quad (1)$$

where $I_0(\lambda)$ is the emitted light flux and $A(\lambda)$ is the absorbance of the solution, and both depend on the wavelength λ . The absorbance is given by the Beer–Lambert equation (Equation (2)):

$$A(\lambda) = l \times c \times \varepsilon(\lambda) \quad (2)$$

where l is the optical pathlength, c is the concentration of the light-absorbing species, and $\varepsilon(\lambda)$ is its molar absorbance. In our system, the photocatalyst is the only species absorbing visible light (in the wavelength range of irradiation), hence, no inner filter effect ought to be taken into account. The photon flux ($I_0(\lambda)$) entering the solution is the product of the total photon flux emitted by the light source ($I_{total}(\lambda)$) and the geometrical factor. The latter one indicates how efficiently the solution (reaction mixture) covers the emission surface of the light source. This factor varies from system to system, depending on the shapes and distances. For the batch reactor, the geometrical factor is 0.9919 (due to its relatively small diameter and high solution level). In the case of the microreactor with winding (serpentine type) channel, its value is 0.003208.

The photon flux absorbed by the reaction mixture (I_{abs}) ought to be divided by its volume (V) to gain suitable parameters for comparison of different reactors. The ratios of these I_{abs}/V values indicate how long an irradiation time is needed for the batch reactor to result in the same photon flux absorbed by a unit of volume as in the case of the microflow reactors at a given flow rate (i.e., residential time). This t_{batch}/t_{micro} ratio for the microflow reactor with ca. rectangular cross-section is 2.213 with the cationic and 1.810 with the anionic porphyrin. Notably, the volume of the solution in the batch reactor is 50 cm³, while in the microreactor it is only 4.15 µL. This three orders of magnitude difference compensates the strongly deviating geometrical factors and optical pathlengths. Hence, the reaction (or residential) times are in the same range. Similarly, for the linear flow reactors (with circular cross-section, see in Table 2), the t_{batch}/t_{micro} ratios are the following: (I) 2.322 and 1.979; (II) 2.174 and 1.886; (III) 2.068 and 1.818 with cationic and anionic porphyrins, respectively.

3. Materials and Methods

3.1. General

All commercial solvents were purchased from Gram Mol (Zagreb, Croatia). Photocatalytic reactions were performed under air atmosphere. The ¹H NMR spectra of photocatalytic products were recorded on a Bruker Avance spectrometer (Coventry, UK) at 600 MHz with CDCl₃ as a solvent and tetramethylsilane as a reference. Column chromatography purifications of products were performed with silica gel (Fluka 60 Å, technical grade, Fluka Chemie GmbH, Buchs, Switzerland). Silica gel 60 F254 (Kieselgel 60, 0.2 mm, 20 × 20 cm, Fluka Chemie GmbH, Buchs, Switzerland) plates were used for thin-layer chromatography (TLC). Organic layers were dried under anhydrous magnesium sulfate (Sigma-Aldrich, St. Louis, MO, USA, SAD). Gas chromatography analysis was performed on a GC-2014 instrument (Shimadzu, Tokio, Japan) with an FID detector and a Zebron ZB-Wax GC capillary column (Phenomenex, Bologna, Italy), 30 m × 0.53 mm, with 1.00 µm film, using nitrogen as carrier gas. The photocatalytic products were analyzed by UPLC with an MS detector equipped with an ESI source (Agilent Technologies, Santa Clara, CA, USA). Experiments of irradiation were performed in a thermostated 50 cm³ cylindrical photoreactor and four different microflow reactors. The initial phosphonium salt was prepared in the laboratory from the corresponding bromide, while the other starting heterocyclic aldehydes used were purchased chemicals (Sigma-Aldrich, St. Louis, MO, USA, SAD). Products of Wittig reaction **1** and **2** as mixtures of *cis*- and *trans*-isomers were used for photocatalytic oxygenation.

3.2. Typical Experimental Procedure for Photocatalytic Oxygenation in Batch Reactor

Heterostilbene derivatives **1** and **2** [34] with oxygen and sulfur heteroatoms were synthesized by the Wittig reaction. The reaction apparatus was purged with nitrogen. In a three-necked flask, phosphonium salt of (4-methylbenzyl)triphenylphosphonium bromide

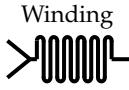
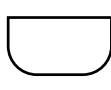
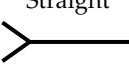
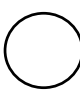
(1 eq, 5.20 mmol; 4.46 mmol) was added to absolute ethanol (100 mL, 3 Å sieves). Then, appropriate heterocyclic aldehyde, in one reaction furan-2-carbaldehyde (1 eq, 5.20 mmol), and in the other thiophene-2-carbaldehyde (1 eq, 4.46 mmol), was added. Finally, the solution of sodium ethoxide (1.1 eq) was added dropwise. The reaction mixture was stirred for 24 h. After the reaction, ethanol was removed by evaporating under reduced pressure. The solid was extracted with toluene p.a. and dried over anhydrous magnesium sulfate. The products were obtained by column chromatography. According to the integrals in UPLC analyses and ^1H NMR spectra, the ratio of isomers of compound **1** was *cis*–:*trans*– = 1:1.3, and for compound **2**, the ratio of isomers was *cis*–:*trans*– = 1:1.2.

Anionic and cationic metalloporphyrins (Mn(III) complexes with *meso*-tetra(4-sulfonatophenyl)porphyrin chloride (MnTSP P^{3-} , acid form) and *meso*-tetra(1-methyl-4-pyridyl)porphyrin pentachloride (MnTMPyP P^{5+}) were used in the experiments of photocatalytic oxygenation. Synthesized 2-(4-methylstyryl)furan **1** and 2-(4-methylstyryl)thiophene **2** and the anionic or cationic Mn(III) porphyrins were dissolved in a solution of 50 cm 3 mixture of acetone/water (50:50) at pH 7. These solutions were irradiated with a 70 W tungsten halogen immersion lamp (Philips, $\lambda_{\text{ir}} > 380$ nm) in a thermostated 50 cm 3 cylindrical photoreactor. During 2 h (furan) and 16 h (thiophene), a stream of air was passed through the solution. Experimental concentration conditions were porphyrins: 1.1×10^{-4} mol dm $^{-3}$ cationic and 9.8×10^{-5} mol dm $^{-3}$ anionic; starting compound **1**: 0.00113 mol dm $^{-3}$, 0.00225 mol dm $^{-3}$, and 0.00450 mol dm $^{-3}$; starting compound **2**: 0.00120 mol dm $^{-3}$, 0.00245 mol dm $^{-3}$, and 0.00490 mol dm $^{-3}$. After irradiation, acetone was evaporated from the reaction mixture. The rest of the solution was extracted with diethylether and dried over magnesium sulfate. Solids were precipitated by evaporating solvent under reduced pressure. In each experiment, the products were detected by TLC. The photocatalytic products **3** (8%, 3 mg), R_f (PE/E 7:3) = 0.71 (from compound **1**, using cationic Mn(III) porphyrin, air saturation), **5** (5%, in traces), R_f (PE/E 7:3) = 0.06 (from compound **1**, using cationic Mn(III) porphyrin, air saturation), **6** (13%, 3.5 mg), R_f (PE/E 7:3) = 0.10 (from compound **1**, using cationic Mn(III) porphyrin, air saturation), **7** (34%, 7 mg), R_f (PE/E 7:3) = 0.08, from compound **1**, using cationic Mn(III) porphyrin, air saturation), **9** (20%, 5 mg/15%, 4 mg), R_f (PE/E 7:3) = 0.67 (from compound **2**, using cationic/anionic Mn(III) porphyrin, air saturation), **11** (10%, 3 mg), R_f (PE/E 7:3) = 0.67 (from compound **2**, using anionic Mn(III) porphyrin, air saturation) were isolated by column chromatography using petroleum ether/diethylether (7:3), but products **4** (23%, 6 mg/24%, 6 mg), R_f (PE/E 7:3) = 0.25 (from compound **1**, using cationic/anionic Mn(III) porphyrin, air saturation), **10** (45%, 8.5 mg/22%, 6 mg), R_f (PE/E 7:3) = 0.83 (from compound **2**, using cationic/anionic Mn(III) porphyrin, oxygen saturation) were isolated by TLC using petroleum ether/diethylether (7:3) as eluent and characterized by spectroscopic methods.

3.3. Experimental Procedure for Photocatalytic Oxygenation in Microflow Reactors

Photocatalytic oxygenation was performed in four different glass microflow reactors. Specific dimensions and volumes are listed in Table 3.

Table 3. Geometric characteristics of microflow reactors.

Microflow Reactor Geometry	Channel Cross Section	Dimensions			
		Height (μm)	50		
		Width (μm)	250		
		Length (mm)	332		
		Volume (μL)	4.15		
			I.	II.	III.
		Radius (μm)	138.09	197.07	248.67
		Length (mm)	166	166	166
		Volume (μL)	9.92	20.25	32.33

All microflow reactors were equipped with Y-shaped input. Two syringe pumps (Harvard Apparatus, Holliston, MA, USA) were used to supply substrate and catalyst in a microflow reactor. The substrate-to-catalyst flow ratio was set to be 1:1 in all experiments to ensure parallel and stable flow from the inlet to the outlet of a microflow reactor. In the experiment performed with rectangular-shaped microflow reactor, due to its specific dimensions, a microflow reactor was placed under the UV lamp (Figure 3b) with a distance from the lamp of 2 mm. Different residence times (from 0.05 to 20 min) were tested to determine the influence of residence time on conversion. When the reaction was performed with circular-shaped microflow reactors, microflow reactors were placed direct to the lamp (Figure 3c). In all experiments, outflows were collected in a vial and samples were analyzed on a gas chromatography and by UPLC/MS analyses.

4. Conclusions

As our results clearly indicated, both the products and the conversion rates in the photocatalytic oxygenation of furo- and thieno heterostilbenes were highly affected by the heteroatom in the aromatic moiety and the charge of the manganese(III) porphyrin catalysts. Due to the stronger aromatic character, the thienyl group proved to be inactive, similarly to the benzene ring. Hence, the reaction rates of the less aromatic, and, thus, less stable, furyl derivative were much higher and its oxygenation resulted in more types of products. The higher reactivity of this compound was also demonstrated by the incorporation of two oxygen atoms in most of the products starting from the furyl derivative **1**, while those originated from the thieno derivative **2** contained only one O. Since these reactions took place via electrophilic attacks by the photogenerated agents such as Mn(V)=O species, higher rates were achieved in the presence of the positively charged photocatalyst. Moreover, the conversion rates could be dramatically increased by the application of microflow reactors, due their favorable geometric features. All these results have unambiguously proved that both the product types and the reaction rates in this system can be efficiently influenced by the application of suitable substrate, catalyst, and reactor.

Author Contributions: The individual contributions are as follows: Conceptualization, I.Š. (Irena Škorić), O.H. and B.Z.; methodology M.M. and A.Š.; formal analysis, I.Š. (Ivana Šagud); investigation, M.B. and M.M.; resources, I.Š. (Irena Škorić), O.H. and B.Z.; writing—original draft preparation, I.Š. (Irena Škorić), A.Š. and O.H.; writing—review and editing, I.Š. (Irena Škorić), O.H. and B.Z.; funding acquisition, I.Š. (Irena Škorić), O.H. and B.Z. All authors have read and agreed to the published version of the manuscript.

Funding: This work was supported by the TKP2020-IKA-07 project financed under the 2020-4.1.1-TKP2020 Thematic Excellence Programme by the National Research, Development and Innovation Fund of Hungary. The University of Zagreb short term scientific support (2020) under the titles *Preparation of new annelated heteropolycyclic systems* and *Integrated microsystems for (photo)chemical synthesis* is also gratefully acknowledged.

Data Availability Statement: The data presented in this study are available on request from the corresponding author. The data are not publicly available due to privacy.

Conflicts of Interest: The authors declare no conflict of interest.

References

1. Wu, D.; Li, Z.; Qi, Z.; Hu, S.; Long, R.; Song, L.; Xiong, Y. Boosting photocatalytic activity in cross-coupling reactions by constructing Pd-oxide heterostructures. *ChemNanoMat* **2020**, *6*, 920–924. [[CrossRef](#)]
2. Huh, S.; Kim, S.-J.; Kim, Y. Porphyrinic metal-organic frameworks from custom-designed porphyrins. *CrystEngComm* **2016**, *18*, 345–368. [[CrossRef](#)]
3. Petrosyan, A.; Hauptmann, R.; Pospech, J. Heteroarene *N*-oxides as oxygen source in organic reactions. *Eur. J. Org. Chem.* **2018**, *38*, 5237–5252. [[CrossRef](#)]
4. De Paula, R.; Simões, M.-M.-Q.; Neves, M.-G.-P.-M.-S.; Cavaleiro, J.-A.-S. Oxidation of styrene and of some derivatives with H₂O₂ catalyzed by novel imidazolium-containing manganese porphyrins: A mechanistic and thermodynamic interpretation. *J. Mol. Catal. A Chem.* **2011**, *345*, 1–11. [[CrossRef](#)]

5. Zhao, X.; Li, B.; Xia, W. Visible-light-promoted photocatalyst-free hydroacylation and diacylation of alkanes turned by $\text{NiCl}_2 \cdot \text{DME}$. *Org. Lett.* **2020**, *22*, 1056–1061. [\[CrossRef\]](#) [\[PubMed\]](#)
6. Wang, B.; Duke, K.; Scaiano, J.-C.; Lanterna, A.-E. Cobalt-molybdenum co-catalyst for heterogeneous photocatalytic H-mediated transformations. *J. Catal.* **2019**, *379*, 33–38. [\[CrossRef\]](#)
7. Firoozi, S.; Hosseini-Sarvari, M. Photo-difunctionalization and photo-oxidative cleavage of the C–C double bond of styrenes in the presence of nanosized Cadmium sulfide (CdS) as a highly efficient photo-induced reusable nanocatalyst. *Eur. J. Org. Chem.* **2020**, *25*, 3834–3843. [\[CrossRef\]](#)
8. Bhadra, M.; Kandambeth, S.; Sahoo, M.-K.; Addicoat, M.; Balaraman, E.; Banerjee, R. Triazine functionalized porous covalent organic framework for photo-organocatalytic E–Z isomerization of olefins. *J. Am. Chem. Soc.* **2019**, *141*, 6152–6156. [\[CrossRef\]](#) [\[PubMed\]](#)
9. Othong, J.; Boonmak, J.; Ha, J.; Leelasubcharoen, S.; Youngme, S. Thermally induced single-crystal-to-single-crystal transformation and heterogeneous catalysts for epoxidation reaction of Co(II) based metal–organic frameworks containing 1,4-phenylenediacetic acid. *Cryst. Growth Des.* **2017**, *17*, 1824–1835. [\[CrossRef\]](#)
10. Webb, D.; Jamison, T.-F. Continuous flow multi-step organic synthesis. *Chem. Sci.* **2010**, *1*, 675–680. [\[CrossRef\]](#)
11. Pastre, J.-C.; Browne, D.-L.; Ley, S.-V. Flow chemistry syntheses of natural products. *Chem. Soc. Rev.* **2013**, *42*, 8849–8869. [\[CrossRef\]](#)
12. Landgraf, S. Application of semiconductor light sources for investigations of photochemical reactions. *Spectrochim. Acta Part A* **2001**, *57*, 2029–2048. [\[CrossRef\]](#)
13. Mešić, A.; Šalić, A.; Gregorić, T.; Zelić, B.; Raić-Malić, S. Continuous flow-ultrasonic synergy in click reactions for the synthesis of novel 1,2,3-triazolyl appended 4,5-unsaturated L-ascorbic acid derivatives. *RSC Adv.* **2017**, *7*, 791–800. [\[CrossRef\]](#)
14. Kikaš, I.; Horváth, O.; Škorić, I. Functionalization of the benzobicyclo[3.2.1]octadiene skeleton via photocatalytic and thermal oxygenation of a furan derivative. *Tetrahedron Lett.* **2011**, *52*, 6255–6259. [\[CrossRef\]](#)
15. Kikaš, I.; Horváth, O.; Škorić, I. Functionalization of the benzobicyclo[3.2.1]octadiene skeleton via photocatalytic oxygenation of furan and benzofuran derivatives. *J. Mol. Struct.* **2013**, *1034*, 62–68. [\[CrossRef\]](#)
16. Vuk, D.; Kikaš, I.; Molčanov, K.; Horváth, O.; Škorić, I. Functionalization of the benzobicyclo[3.2.1]octadiene skeleton via photocatalytic oxygenation of thiophene and furan derivatives: The impact of the type and position of the heteroatom. *J. Mol. Struct.* **2014**, *1063*, 83–91. [\[CrossRef\]](#)
17. Šagud, I.; Škorić, I. Photocatalytic oxygenation by water-soluble metalloporphyrins as a pathway to functionalized polycycles. *Int. J. Photoenergy* **2018**, *2018*, 1–8. [\[CrossRef\]](#)
18. Vuk, D.; Horváth, O.; Škorić, I. New functionalized polycycles obtained by photocatalytic oxygenation using Mn(III) porphyrins in basic media. *Catalysts* **2019**, *9*, 304. [\[CrossRef\]](#)
19. Hennig, H.; Lippa, D. Photocatalytic activation of oxygen by iron(III) porphyrins. *J. Für Prakt. Chem.* **1999**, *341*, 757–767. [\[CrossRef\]](#)
20. Hennig, H. Homogeneous photo catalysis by transition metal complexes. *Coord. Chem. Rev.* **1999**, *182*, 101–123. [\[CrossRef\]](#)
21. Hajimohammadi, M.; Bahadoran, F.; Davarani, S.-S.-H.; Safari, N. Selective photocatalytic epoxidation of cyclooctene by molecular oxygen in the presence of porphyrin sensitizers. *React. Kinet. Mech. Catal.* **2009**, *99*, 243–250. [\[CrossRef\]](#)
22. Zhang, R.; Horner, J.-H.; Newcomb, M. Laser flash photolysis generation and kinetic studies of porphyrin-manganese-oxo intermediates. Rate constants for oxidations effected by porphyrin-Mn(V)-oxo species and apparent disproportionation equilibrium constants for porphyrin-Mn(IV)-oxo species. *J. Am. Chem. Soc.* **2005**, *127*, 6573–6582. [\[CrossRef\]](#)
23. Newcomb, M.; Zhang, R.; Pan, Z.; Harischandra, D.; Chandrasena, R.; Horner, J.; Martinez II, E. Laser flash photolysis production of metal-oxo derivatives and direct kinetic studies of their oxidation reactions. *Catal. Today* **2006**, *117*, 98–104. [\[CrossRef\]](#)
24. Zhang, R.; Newcomb, M. Laser flash photolysis generation of high-valent transition metal-oxo species: Insights from kinetic studies in real time. *Acc. Chem. Res.* **2008**, *41*, 468–477. [\[CrossRef\]](#) [\[PubMed\]](#)
25. Hennig, H.; Behling, J.; Meusinger, R.; Weber, L. Photocatalytic oxygenation of selected cycloalkenes in aqueous solutions induced by water-soluble metal porphyrin complexes. *Chem. Ber.* **1995**, *128*, 229–234. [\[CrossRef\]](#)
26. Baglia, R.-A.; Zaragoza, J.-P.-T.; Goldberg, D.-P. Biomimetic reactivity of oxygen-derived manganese and iron porphyrinoid complexes. *Chem. Rev.* **2017**, *117*, 13320–13352. [\[CrossRef\]](#) [\[PubMed\]](#)
27. Harris, T.-K.; Keshwani, M.-M. Measurement of enzyme activity. In *Guide to Protein Purification*, 2nd ed.; Burgess, R.-R., Deutcher, M.-P., Eds.; Biochemistry & Molecular Biology, University of Miami School of Medicine: Miami, FL, USA; Elsevier: San Diego, CA, USA, 2009; Volume 463, pp. 57–71.
28. Cambié, D.; Bottecchia, C.; Straathof, N.J.W.; Hessel, V.; Noël, T. Applications of Continuous-Flow Photochemistry in Organic Synthesis, Material Science, and Water Treatment. *Chem. Rev.* **2016**, *116*, 10276–10341. [\[CrossRef\]](#)
29. Talla, A.; Driessen, B.; Straathof, N.J.W.; Milroy, L.-G.; Brunsveld, L.; Hessel, V.; Noel, T. Metal-free photocatalytic aerobic oxidation of thiols to disulfides in batch and continuous-flow. *Adv. Synth. Catal.* **2015**, *357*, 2180–2186. [\[CrossRef\]](#)
30. Maeda, H.; Mukae, H.; Mizuno, K. Enhanced efficiency and regioselectivity of intramolecular ($2\pi + 2\pi$) photocycloaddition of 1-cyanonaphthalene derivative using microreactors. *Chem. Lett.* **2005**, *34*, 66–67. [\[CrossRef\]](#)
31. Finn, P.B.; Kulyk, S.; Sieburth, S.M. Formation and isomerization of polycyclic 1,5-enynes. *Tetrahedron Lett.* **2015**, *56*, 3567–3570. [\[CrossRef\]](#)
32. Tsutsumi, K.; Terao, K.; Yamaguchi, H.; Yoshimura, S.; Morimoto, T.; Kakiuchi, K.; Fukuyama, T.; Ryu, I. Diastereoselective [2 + 2] photocycloaddition of chiral cyclic enone and cyclopentene using a microflow reactor system. *Chem. Lett.* **2010**, *39*, 828–829. [\[CrossRef\]](#)

-
33. Terao, K.; Nishiyama, Y.; Aida, S.; Tanimoto, H.; Morimoto, T.; Kakiuchi, K. Diastereodifferentiating [2 + 2] photocycloaddition of chiral cyclohexenone carboxylates with cyclopentene by a microreactor. *J. Photochem. Photobiol. A* **2012**, *242*, 13–19. [[CrossRef](#)]
 34. Qu, J.; Cao, C.T.; Cao, C. Determining the excited-state substituent constants of furyl and thienyl groups. *J. Phys. Org. Chem.* **2018**, *31*, 3799. [[CrossRef](#)]